

# Double photoionization of helium: The hyperspherical $\mathcal{R}$ -matrix method with semiclassical outgoing waves

L. Malegat and P. Selles

*Laboratoire de Spectroscopie Atomique et Ionique (Laboratoire Associé au CNRS), Université Paris-Sud, Batiment 350, 91405 Orsay Cedex, France*

A. Kazansky

*Institute of Physics, The University of St. Petersburg, St. Petersburg, 198904 Russia*

(Received 18 February 1999)

We present an *ab initio* scheme for computing the wave function of the pair of electrons projected into the double continuum of the helium atom by a one-photon dipolar excitation. The scheme uses the Floquet approach to convert the time-dependent Schrödinger equation into an infinite set of coupled time-independent equations. The latter reduces to a single stationary inhomogeneous Schrödinger equation in the weak-field limit, which is relevant here. This equation is solved using an  $\mathcal{R}$  matrix approach to combine a quantum treatment of all variables within the hypersphere  $R \leq R_0$  with a semiclassical treatment of the  $R$  motion outside this hypersphere. We apply this approach to a model helium atom where  $r_1 = r_2$ . We thus demonstrate the feasibility of the method, and obtain insights into the dynamics of the double photoionization of helium at equal sharing of a low excess energy. [S1050-2947(99)01210-X]

PACS number(s): 32.80.Fb

## I. INTRODUCTION

Double photoionization (DPI) of He, though an elementary process of atomic physics, remains a challenge for experimentalists as well as for theoreticians. This paradox results from the DPI process being entirely due to the electronic correlations in the initial and in the final state. Experimentalists are then faced with the measurement of a very low signal, and theoreticians are faced with the nonperturbative description of a correlated motion not only in a bound but also in a continuum state.

The interest in this low rate photoprocess has been boosted in recent years by the great improvements of the experimental tools, namely the advent of second- and third-generation synchrotron facilities delivering intense photon beams, as well as the development of position-sensitive detectors with high spatial and temporal resolution. Accordingly, detailed information on the most challenging case of near-threshold DPI of He has become recently available and is still under progress right now [1–3].

Important advances have been achieved on the theoretical side as well. However, no single method has yet been recognized as providing a definitive description of the process.

This is because most methods used so far rely upon extending to DPI the numerical schemes designed for single photoionization studies: one looks for a solution of the stationary homogeneous Schrödinger equation satisfying the appropriate photoionization boundary condition. But for double ionization, this condition becomes very difficult both to formulate and to enforce: the asymptotic form of the wave function itself is still the object of intensive research [4–7], and its matching to an accurate short-range  $L^2$  solution has not been accomplished yet. One is then led to introduce approximations: in fact, most approaches eligible in the near-threshold domain extend over the entire configuration space a representation of the wave function which is valid only

within a restricted region. This restricted region turns out to be the asymptotic region, in methods based on three-body Coulomb asymptotic wave functions [8–10], or, inversely, the short-range region, in  $L^2$  methods [11–13], or else the neighborhood of the saddle point of the three-body potential surface in methods [14–23] which make use of the Wannier [24] analysis.

New promising approaches have emerged recently, where these difficulties are avoided by relying, explicitly or implicitly, upon the time-dependent Schrödinger equation. In [25], the time-dependent Schrödinger equation is solved directly, but the cross sections are not extracted from the final wave packet yet. In [26–31], the authors consider the stationary inhomogeneous equation, which can be deduced from the latter by taking the wave packet in the Floquet form.

The approach we present in this paper belongs to this very last class of methods. It is described in Sec. II. In Sec. III, a numerical scheme is proposed to solve the resulting equations. In Sec. IV, we apply it to a model helium atom where the two electrons remain at equal distances from the core. We present our conclusions, along with directions for future work, in Sec. V. In the following, we use atomic units for the mechanical quantities and Gaussian units for the electromagnetic ones.

## II. THEORETICAL FRAME

Let us consider a helium atom in the ground state  $\Psi_0$  with energy  $E_0$  of its Hamiltonian  $H_0$ . At time  $t=0$ , we switch on an external field which oscillates at the frequency  $\omega$ . The atom-field interaction  $V(t)$  oscillates with the same frequency. The further evolution of the atomic wave function  $\Psi$  is governed by the time-dependent Schrödinger equation

$$i \frac{\partial \Psi}{\partial t} = [H_0 + V(t)] \Psi(t). \quad (1)$$

According to Floquet's theorem (see [32] and references therein), the solution of Eq. (1) can be searched for, with no loss of generality, in the form of a phase factor  $\exp(-i\mathcal{E}t)$ , involving a "quasienergy"  $\mathcal{E}$ , times a periodic function of time  $\Phi(t)$  with the period  $T=2\pi/\omega$ . By expanding  $\Phi(t)$  and  $V(t)$  in Fourier series

$$V(t) = \sum_{k=-\infty}^{+\infty} V_k e^{-ik\omega t}, \quad (2a)$$

$$\Psi(t) = e^{-i\mathcal{E}t} \Phi(t) = e^{-i\mathcal{E}t} \sum_{n=-\infty}^{+\infty} \Phi_n e^{-in\omega t}, \quad (2b)$$

the original time-dependent problem is turned into the infinite set of coupled stationary equations

$$(\mathcal{E} + n\omega - H_0)\Phi_n = \sum_{k=-\infty}^{+\infty} V_k \Phi_{n-k}, \quad n = -\infty, \dots, +\infty, \quad (3a)$$

$$\sum_{n=-\infty}^{+\infty} \Phi_n = \Psi_0. \quad (3b)$$

Extensive use has been made of the Floquet equations (3) for the study of multiphoton processes in intense laser fields [33]. But they can shed light as well on the weak-field case where one-photon absorption is the only relevant process. Then,  $n$  runs only from 0 to 1 and  $k$  reduces to the single value  $+1$ , so that Eq. (3) reduces to a system of three coupled equations involving the three unknown quantities  $\mathcal{E}, \Phi_0, \Phi_1$ . To lowest order in the field, the solution is obtained by setting  $\Phi_0 \approx \Psi_0$  and  $\mathcal{E} \approx E_0$ , so that  $\Phi_1$  satisfies the stationary inhomogeneous equation

$$(E_0 + \omega - H_0)\Phi_1 = V_{+1}\Psi_0. \quad (4)$$

An outgoing wave boundary condition is appropriate for this Fourier component of the wave packet (2b). Equation (4), which is central to our approach, has already been used in previous photon- or electron-impact ionization studies [29–31, 26–28].

We specialize here on the case where the final energy  $E = E_0 + \omega$  lies above the double ionization threshold. In this case, the behavior of  $\Phi_1$  in the region of configuration space where *both*  $r_1$  and  $r_2$  tend to infinity reflects the dynamics of the double escape process. By contrast, its behavior where *either*  $r_1$  or  $r_2$  tends to infinity corresponds to the competing process of single escape. We focus here on the double ionization process which is best described using as coordinates the hyperspherical radius  $R = \sqrt{r_1^2 + r_2^2}$ , the hyperangle  $\alpha = \arctan(r_1/r_2)$ , and a set  $\Omega_4$  of four angles specifying the directions of the two electrons, with  $\Omega_5$  denoting the set  $\{\alpha, \Omega_4\}$  as often as possible, for compactness. The asymptotic behavior of  $\Phi_1$  corresponding to double escape can then be quantified [34] as

$$\lim_{R \rightarrow \infty} \Phi_1(R, \Omega_5) = \frac{e^{iKR + i\xi(\Omega_5)\ln(KR)}}{R^{5/2}} F(\Omega_5), \quad \alpha \neq 0, \pi/2. \quad (5)$$

In Eq. (5),  $K$  is the module of the six-dimensional asymptotic momentum  $\vec{K} = (\mathbf{k}_1, \mathbf{k}_2)$  defined from the three-dimensional asymptotic momenta  $\mathbf{k}_1$  and  $\mathbf{k}_2$  of the two electrons. The function  $\xi(\Omega_5)$  is given by  $Z/k_1 + Z/k_2 - 1/|\mathbf{k}_1 - \mathbf{k}_2|$ , where  $Z$  is the nuclear charge, namely  $Z=2$ . The function  $F(\Omega_5)$  is the double photoionization amplitude. The asymptotic six-dimensional current associated to  $\Phi_1$  is given to lowest order in  $1/R$  by  $\vec{J} = K|\Phi_1|^2 \vec{R}/R$ , where  $\vec{R} = (\mathbf{r}_1, \mathbf{r}_2)$ . Now we set  $\Omega_4 = \{\Omega_1, \Omega_2\} = \{(\theta_1, \varphi_1), (\theta_2, \varphi_2)\}$ , where  $(\theta_1, \varphi_1)$  and  $(\theta_2, \varphi_2)$  are the spherical angles of the asymptotic momenta  $\mathbf{k}_1$  and  $\mathbf{k}_2$ , and we introduce the asymptotic kinetic energies  $E_1$  and  $E_2$  of the two electrons, which satisfy  $E_1 + E_2 = E$  and  $E_1/E_2 = \tan^2 \alpha$ . The surface element on the hypersphere  $\Sigma_R$  of hyperradius  $R$  can then be written  $d\vec{S} = R^5 \sin 2\alpha dE_1 d\Omega_1 d\Omega_2 \vec{R}/4ER$ , so that the asymptotic flux  $\mathcal{F}_{\text{out}} = \int_{\Sigma_\infty} \vec{J} \cdot d\vec{S}$  of  $\vec{J}$  through a hypersphere of infinite hyper-radius reads

$$\mathcal{F}_{\text{out}} = \frac{K}{4E} \lim_{R \rightarrow \infty} \int_{\Sigma_R} R^5 |\Phi_1|^2 \sin 2\alpha dE_1 d\Omega_1 d\Omega_2. \quad (6)$$

The total double ionization cross section  $\sigma_{(\gamma, 2e)}$ , defined as the ratio of  $\mathcal{F}_{\text{out}}$  to the incoming photon flux  $\mathcal{F}_{\text{in}}$ , is independent of the amplitude of the electric field associated with the incident plane electromagnetic wave. Accordingly, we assume the latter to be unity, so that  $\mathcal{F}_{\text{in}} = c/8\pi\omega$  with  $c$  the speed of light, and we get

$$\sigma_{(\gamma, 2e)} = \frac{2\pi\omega K}{cE} \lim_{R \rightarrow \infty} \int_{\Sigma_R} R^5 |\Phi_1|^2 \sin 2\alpha dE_1 d\Omega_1 d\Omega_2. \quad (7)$$

The expressions of the various differential cross sections follow, with the triple differential cross section (TDCS), for instance, being given by

$$\sigma_{(\gamma, 2e)}^{(3)}(E_1, \Omega_1, \Omega_2) = \frac{2\pi\omega K}{cE} \lim_{R \rightarrow \infty} R^5 |\Phi_1|^2 \sin 2\alpha. \quad (8)$$

The limits in Eqs. (7) and (8) are easily taken by replacing  $R^5 |\Phi_1|^2$  by  $|F(\Omega_5)|^2$  according to Eq. (5). Computing the various DPI cross sections then amounts to solving Eq. (4) subject to the outgoing wave boundary condition up to very large  $R$ . At this point, it is convenient to write down the right-hand side of Eq. (4) explicitly in the dipole approximation. Assuming, with no loss of generality, that the unit electric field is directed along the  $z$  axis, we get

$$V_{+1}\Psi_0 = [T(\vec{r}_1) + T(\vec{r}_2)]\Psi_0, \quad (9)$$

where the dipole transition operator  $T(\vec{r})$  assumes different forms in the length ( $L$ ), the velocity ( $V$ ), or the acceleration ( $A$ ) gauges:

$$T^L(\vec{r}) = \frac{1}{2}z, \quad (10a)$$

$$T^V(\vec{r}) = \frac{1}{2\omega} \frac{\partial}{\partial z}, \quad (10b)$$

$$T^A(\vec{r}) = \frac{Z}{2\omega^2} \frac{z}{r^3}. \quad (10c)$$

Note that, when acting on a fully symmetric  $^1S^e$  state,  $T(\vec{r})$  in Eq. (9) can be replaced in the  $V$  gauge by

$$T^V(\vec{r}) = \frac{1}{2\omega} \frac{z}{r} \frac{\partial}{\partial r}. \quad (11)$$

The physical results being invariant if the right-hand side of Eq. (4)—and hence  $\Phi_1$ —is multiplied by an arbitrary phase factor, we have taken positive signs on the right-hand side of each member of Eq. (10), for simplicity. Note that, although the right-hand side of Eq. (4) has a gauge-dependent form, the solution  $\Phi_1$  must be gauge independent.

To conclude, let us stress that this theoretical formulation, based on a *stationary inhomogeneous* equation, combines the advantages of a nonstationary approach, where the difficulties of defining and imposing a double photoionization asymptotic condition are avoided, with those of a stationary homogeneous approach, where optimized numerical methods have long been available.

### III. NUMERICAL SCHEME

#### A. A short sketch

Basic to our scheme is the splitting of configuration space into an inner region  $R \leq R_0$  and an outer region  $R > R_0$ . In the inner region, we apply a quantum treatment to all dynamical variables including  $R$ . In the outer region, by contrast, we restrict the quantum treatment to the angular variables  $\Omega_5$ , and treat  $R$  semiclassically. Accordingly, we must take  $R_0$  large enough for the semiclassical treatment of the  $R$  motion to be valid in the external region.

Using the  $\mathcal{R}$  matrix technique [35] in the inner region, we derive from Eq. (4) a linear inhomogeneous relation between the values of some set of radial channel functions  $f_j(R)$  and the values of their derivatives  $f'_j(R)$  at the boundary  $R_0$ . Let us emphasize that here, unlike in standard  $\mathcal{R}$  matrix treatments, the derivatives are taken with respect to the hyperradius  $R$  instead of the radius of a single outgoing particle. In addition, due to the right-hand side in Eq. (4), the  $\mathcal{R}$  matrix condition becomes inhomogeneous. Next, we perform a frame transformation to locally adapted angular partial waves [36] at  $R_0$ : the locally uncoupled radial channel functions  $F_j(R)$  which result in the adiabatic approximation satisfy the frame transformed  $\mathcal{R}$  matrix condition. Again,  $R_0$  must be taken large, so that the adiabatic approximation is valid from  $R_0$  outwards.

To these uncoupled radial channel functions we impose the behavior of outgoing semiclassical waves: a linear homogeneous relation follows between the  $F_j(R)$  and their derivatives  $F'_j(R)$  at any  $R \geq R_0$ .

Next, we solve the two independent linear relations obtained so far for the radial channel functions  $F_j(R_0)$  at the boundary, and we construct the full wave function  $\Phi_1(R_0, \Omega_5)$ . We are then left with the task of propagating it outwards in  $R$  using the appropriate semiclassical scheme.

To summarize, the originality of this scheme lies in the combination of the  $\mathcal{R}$  matrix technique with the semiclassi-

cal approximation in the outer region using the hyperspherical radius as the matching coordinate. The following sections give the detailed equations.

#### B. The inner region equations

Let us first rewrite Eq. (4) more explicitly. Inserting  $\Phi_1(R, \Omega_5) = (R^{5/2} \sin 2\alpha)^{-1} \Phi(R, \Omega_5)$  and premultiplying by  $-R^{5/2} \sin 2\alpha$ , we get

$$\left( -\frac{1}{2} \frac{\partial^2}{\partial R^2} + T_{\Omega_5} + V(R, \Omega_5) - E \right) \Phi(R, \Omega_5) = \Phi^G(R, \Omega_5). \quad (12)$$

The first two terms on the left-hand side describe the kinetic energy of the system, with the radial contribution singled out. The next term is the three-body interaction potential

$$V(R, \Omega_5) = -\frac{Z}{r_1} - \frac{Z}{r_2} + \frac{1}{r_{12}}, \quad (13)$$

and the right-hand side  $\Phi^G(R, \Omega_5) = -R^{5/2} \sin 2\alpha V_{+1} \Psi_0$  can be made explicit using Eqs. (9)–(11). Following the  $\mathcal{R}$  matrix technique, we consider now the real eigenvalues  $E_k$  and the associated orthonormal eigenvectors  $\Phi^k(R, \Omega_5)$  of the left-hand side operator in Eq. (12) completed by the Bloch term [37] required to ensure that it is Hermitian over the finite inner region. They satisfy

$$\left( -\frac{1}{2} \frac{\partial^2}{\partial R^2} + \frac{1}{2} \delta(R - R_0) \frac{\partial}{\partial R} + T_{\Omega_5} + V(R, \Omega_5) - E_k \right) \times \Phi^k(R, \Omega_5) = 0, \quad R \leq R_0. \quad (14)$$

Then, we premultiply Eq. (12) by  $\Phi^{k*}$ , Eq. (14) by  $\Phi^*$ , subtract the complex conjugate of the latter from the former, and integrate over the inner region with the volume element now given by  $dR d\Omega_5 = dR d\alpha d\Omega_4/4$  due to the change of unknown functions performed. The contributions of the potential  $V(R, \Omega_5)$  cancel each other. Those of the Hermitian operator  $T_{\Omega_5}$  cancel each other as well. The remaining terms are computed by expanding  $\Phi$  and the  $\Phi^k$  into partial waves as

$$\Phi(R, \Omega_5) = \sum_m f_m(R) x_m(\Omega_5), \quad (15a)$$

$$\Phi^k(R, \Omega_5) = \sum_m f_m^k(R) x_m(\Omega_5). \quad (15b)$$

Observing that the radial functions in Eqs. (15) vanish at least as quickly as  $R^{5/2}$  as  $R$  tends to zero, and assuming that the  $\Phi^k$  form a complete orthonormal basis over the finite inner region, we get the announced  $\mathcal{R}$  matrix type relation

$$f = \mathcal{R}f' + \mathcal{I}, \quad (16a)$$

$$\mathcal{I}_m(R_0) = \sum_k \frac{\langle \Phi^k | \Phi^G \rangle}{E_k - E} f_m^k(R_0), \quad (16b)$$

$$\mathcal{R}_{mm'}(R_0) = \frac{1}{2} \sum_k \frac{f_m^k(R_0) f_{m'}^{k*}(R_0)}{E_k - E}. \quad (16c)$$

### C. The outer region equations

Let us now introduce, at any fixed hyperradius  $R$  in the outer region, the locally adapted angular basis set  $\{X_M(R; \Omega_5)\}$  defined by

$$[T_{\Omega_5} + V(R, \Omega_5) - E_M(R)] X_M(R; \Omega_5) = 0, \quad R \geq R_0. \quad (17)$$

Note that our notation distinguishes the dependence of the  $X_M$  on the angles  $\Omega_5$  from their parametric dependence on  $R$ , which is expected to be smooth at large  $R$ . This new basis is related to the original one by a unitary transformation, which also connects the original radial channel functions to the new ones denoted  $F_M(R)$ . This is expressed in matrix notation as

$$X(R; \Omega_5) = U(R) x(\Omega_5), \quad (18a)$$

$$F(R) = U(R) f(R). \quad (18b)$$

In deriving the new radial equations from Eq. (12), we introduce the following outer region approximations: (i) we neglect the inhomogeneous term, which decays exponentially with increasing  $R$ ; (ii) we neglect the nonadiabatic couplings due to the parametric radial dependence of the  $X_M$ . We get then

$$\left( -\frac{1}{2} \frac{\partial^2}{\partial R^2} + E_M(R) - E \right) F_M(R) = 0, \quad (19)$$

which shows that the new channels are uncoupled, with the radial motion in each channel governed by the channel adiabatic potential. This situation lends itself particularly well to the implementation of the semiclassical approximation defined by

$$F_M(R) = \frac{1}{\sqrt{|p_M(R)|}} e^{i \int_{R_0}^R p_M(R') dR'} \tilde{F}_M(R), \quad (20a)$$

$$p_M(R) = \sqrt{2[E - E_M(R)]}, \quad (20b)$$

$$\frac{d^2 \tilde{F}_M}{dR^2} \ll 1 \quad \text{and} \quad \left| \frac{1}{p_M^2} \frac{dp_M}{dR} \right| \ll 1. \quad (20c)$$

The relations (20) ensure an outgoing behavior in the open channels and an exponentially decaying behavior in the closed channels, in agreement with the physical meaning of the wave function  $\Phi$ . In addition, a relation of proportionality is obtained between  $F_M$  and  $F'_M$ , which can be written in matrix form as

$$F' = i p F, \quad (21)$$

where  $p$  is the diagonal matrix of the semiclassical momenta in each channel.

### D. Matching

Letting  $U(R_0)$  act on Eq. (16a), expressing the continuity of the wave function and its first radial derivative at the boundary, and taking account of the proportionality relation given by Eq. (21) at  $R_0$ , we get the following set of linear inhomogeneous equations for the  $F_M(R_0)$ :

$$(i p U R U^\dagger p - p) F = -p U \mathcal{I} \quad \text{at } R = R_0. \quad (22)$$

Once we have solved Eq. (22), we can set up the full wave function  $\Phi_1(R_0, \Omega_5)$  at the boundary. Its knowledge is enough to initiate a semiclassical radial propagation up to as large a hyperradius as needed.

To summarize, our method sets up  $\Phi_1(R_0, \Omega_5)$  by combining a quantum treatment of all angular variables  $\Omega_5$  with a specific treatment of the hyperradius  $R$ , based on quantum mechanics in the inner region, but on the semiclassical approximation in the outer region. By completing it with the semiclassical propagation scheme, we can obtain  $\Phi_1(R_\infty, \Omega_5)$ , and accordingly the observable cross sections. The matching radius  $R_0$  must be chosen large enough for the semiclassical and adiabatic approximations to be valid in the external region. The originality of our approach, compared to previous ones based on the same stationary inhomogeneous equation [26–31], is that the solution of the latter satisfying the appropriate outgoing wave boundary condition is obtained over the entire configuration space, that is to say, from the inner reaction zone up to the asymptotic region, where the cross sections can be extracted directly.

## IV. FIRST APPLICATION

### A. The $\alpha = \pi/4$ model

We wanted to perform a quick test of our method on a current desk computer. This is why we have searched for a model problem of reduced dimensionality to apply it to.

The pioneering work of Wannier [24] is at the origin of many such models for the near-threshold double photoionization of two electron atoms. Wannier considered the classical motion of the representative point  $(R, \alpha, \theta_{12})$  of a two-electron  $S$  state, which is determined, at very low energy, by the structure of the three-body potential surface  $V(R, \alpha, \theta_{12})$ —with the obvious notation  $\theta_{12} = (\mathbf{k}_1, \mathbf{k}_2)$ . Basing his argument on the well known saddle shape of this surface at fixed  $R$ , as well as on the dissipative character of the equations of a related simulated system, he concluded that all trajectories leading to double escape pass, at some critical radial distance, through the eye of a needle set out at the saddle point ( $\alpha = \pi/4, \theta_{12} = \pi$ ). The idea followed that many features of near-threshold double escape could be obtained from a study of the dynamics in the neighborhood of the saddle point, where the unstable  $\alpha$  motion decouples from the stable  $\theta_{12}$  motion. This decoupling was later extended beyond the vicinity of the saddle point in semiclassical studies of the motion at fixed  $\alpha = \pi/4$  and free  $\theta_{12}$  [extended Wannier ridge model (EWRM) [30,31]].

By analogy with EWRM studies, we restrict our general approach by setting  $\alpha = \pi/4$ , to define a first testing bench of reduced dimensionality for our method. As a result, our calculations will only concern the equal energy sharing situation, since  $E_1/E_2 = \tan^2 \alpha$ .

### B. Numerical implementation

The main tasks in our method are (i) to solve the inner region eigenvalue equation (14) for eigenvectors expanded in angular partial waves according to Eq. (15); (ii) to compute the overlaps  $\langle \Phi^k | \Phi^G \rangle$  of the right-hand side of Eq. (12) with these eigenvectors over the finite inner region; and (iii) to solve the fixed  $R$  eigenvalue equation (17) at the boundary, which is merely a particular case of (i). Once these tasks are completed, the  $\mathcal{R}$  matrix and  $\mathcal{I}$  vector can be assembled according to Eq. (16), the matrix  $p$  of the semiclassical momenta can be set up from Eq. (20), and the unitary matrix  $U$  is readily available. It is then straightforward to solve Eq. (22) for the wave function at the boundary.

To make clear how these tasks are performed within the present model, we first complete the specification of the coordinate system. Since  $\alpha = \pi/4$ ,  $\Omega_5$  reduces to  $\Omega_4$ , which we write as  $\Omega_4 = \{\theta_{12}, \Omega_3\}$ , where  $\Omega_3$  is the set of three Euler angles associated with the rotation, which takes the laboratory frame  $Oxyz$  into the body fixed frame  $OXYZ$  such that  $\hat{Z} \propto \hat{\mathbf{r}}_1 \times \hat{\mathbf{r}}_2$  and  $\hat{\mathbf{X}} \propto \hat{\mathbf{r}}_1 + \hat{\mathbf{r}}_2$  as in [38]. With these coordinates the differential operator  $T_{\Omega_5}$  reduces to

$$T_{\Omega_5} = \frac{1}{2R^2} \left( L^2 + \ell^2 - \frac{1}{4} \right), \quad (23)$$

where  $\mathbf{L} = \ell_1 + \ell_2$  is the total angular momentum of the electron pair, acting on  $\Omega_3$ , and  $\ell = \ell_1 - \ell_2$  is the relative angular momentum of the two electrons, which acts on  $\theta_{12}$  as well. Detailed expressions of these operators in this coordinate system can be found in [38].

Next we choose a partial wave representation  $x_m(\Omega_4)$ . Let us first recall that, when  $\alpha$  is frozen at its saddle point value  $\pi/4$ , the  ${}^1P^o$  wave function  $\Phi^k(R, \Omega_4)$  can be written in full generality [38,39] as the product of a function  $\phi^k(R, \theta_{12})$  by a symmetrized Wigner function  $D_{01}^{1+}(\Omega_3)$  [39,40]. The latter can be expressed in terms of  $\theta_{12}$  and of the polar angles  $\theta_1$  and  $\theta_2$  of  $\mathbf{k}_1$  and  $\mathbf{k}_2$  in the laboratory frame as

$$D_{01}^{1+}(\Omega_3) = -\frac{\cos \theta_1 + \cos \theta_2}{2 \cos \frac{\theta_{12}}{2}}. \quad (24)$$

At this stage, it is convenient to eliminate the Euler angles from the dynamical treatment, to get rid of the  $R^{-2}$  singularity due to  $T_{\Omega_5}$  in Eq. (14), and to work on a standard inner region of unit hyperradius. This is accomplished by introducing the scaled hyperradius  $r = R/R_0$ , setting

$$\Phi^k(R, \Omega_4) = R_0 r \varphi^k(r, \theta_{12}) D_{01}^{1+}(\Omega_3), \quad (25)$$

premultiplying Eq. (14) by  $R_0 r$ , and finally projecting it on  $D_{01}^{1+}(\Omega_3)$ . We then arrive at

$$\left[ -\frac{1}{2} r \frac{\partial^2}{\partial r^2} r + \frac{1}{2} \delta(r-1) \left( 1 + \frac{\partial}{\partial r} \right) + 4t^{\theta_{12}} + \frac{3}{8} - 2Z\sqrt{2}R_0 r \right. \\ \left. + R_0 r W(\theta_{12}) - R_0^2 r^2 E_k \right] \varphi^k(r, \theta_{12}) = 0, \quad 0 \leq r \leq 1, \quad (26)$$

with the following definitions for the angular operators:

$$t^{\theta_{12}} = -\frac{1}{2 \sin \theta_{12}} \frac{\partial}{\partial \theta_{12}} \sin \theta_{12} \frac{\partial}{\partial \theta_{12}} - \frac{\cos \theta_{12} - 1}{4 \sin^2 \theta_{12}}, \quad (27a)$$

$$W(\theta_{12}) = \frac{1}{\sqrt{1 - \cos \theta_{12}}}. \quad (27b)$$

We now complete our partial wave representation by choosing as a  $\theta_{12}$  basis the set of orthonormal vectors

$$g_{\ell}(\theta_{12}) = \sqrt{\ell+1} d_{1/2,1/2}^{\ell+1/2}(\theta_{12}) = \sqrt{\ell+1} \cos \frac{\theta_{12}}{2} P_{\ell}^{01}(\cos \theta_{12}). \quad (28)$$

The function  $\varphi^k(r, \theta_{12})$  must contain a  $\cos(\theta_{12}/2)$  factor to cancel the  $[\cos(\theta_{12}/2)]^{-1}$  term in  $D_{01}^{1+}(\Omega_3)$  and to let the well-known node of the  ${}^1P^o$  wave function at  $\theta_{12} = \pi$  appear. Besides, the Jacobi polynomials  $P_{\ell}^{01}(\cos \theta_{12})$  form a complete basis for any function of  $\theta_{12}$ . Accordingly, the  $g_{\ell}(\theta_{12})$ ,  $\ell = 0, \dots, \ell_{\max}$  form a complete basis for the  $\theta_{12}$  dependence of  $\varphi^k(r, \theta_{12})$ . In addition, they are eigenvectors of  $t^{\theta_{12}}$  with the eigenvalues  $(2\ell+1)(2\ell+3)/8$  [40], so that they provide, without any calculation, the required Hermitian representation of  $t^{\theta_{12}}$ . They also allow the matrix elements of  $W(\theta_{12})$  to be computed exactly using low-order Gauss Legendre quadratures. To summarize, our partial wave representation is given by

$$x_{\ell}(\Omega_4) = \sqrt{\ell+1} \cos \frac{\theta_{12}}{2} P_{\ell}^{01}(\cos \theta_{12}) D_{01}^{1+}(\Omega_3), \quad (29)$$

where  $\ell$  is connected with the relative angular momentum of the electron pair and varies from 0 to  $\ell_{\max}$ .

To solve the system of coupled radial differential equations obtained by restricting Eq. (26) to the subspace spanned by the  $g_{\ell}(\theta_{12})$ , we project it on the radial basis formed by the  $n$  normalized Lagrange functions

$$h_i(r) = (-1)^i \sqrt{r_i(1-r_i)} \frac{(2n+3)!!}{n!(n+3)!} r^{3/2} \frac{G_n^{44}(r)}{r-r_i}, \quad (30)$$

associated to the shifted Jacobi polynomial  $G_n^{44}(r)$  of degree  $n$  with  $n$  zeros  $r_i, i = 1, 2, \dots, n$  within the interval of definition  $[0,1]$  [see [41] for the original presentation of the Lagrange mesh method, which is a particularly convenient formulation of the better known discrete variable representation (DVR) [42]]. These functions, which form an orthonormal basis, display the appropriate behavior at both ends of the definition interval: they vanish as  $r^{3/2}$  at  $r=0$  and take nonzero values at  $r \approx 1$ , thus allowing a loss of flux through the hypersurface  $R=R_0$ . The associated representation is most accurate near 0 and 1, where the zeros of the Jacobi polynomial are accumulated: these are the important regions in our treatment, since the  $\mathcal{R}$  matrix condition, expressed at  $r=1$ , involves the scalar products  $\langle \Phi^k | \Phi^G \rangle$  of the  $\Phi^k$  with the short-range  $\Phi^G$ . In addition, exact analytical expressions can be obtained for the matrix elements of all radial operators, in accordance with the general property of the Lagrange mesh method (see, for instance, [43]).

The computation of the overlaps  $\langle \Phi^k | \Phi^G \rangle$  involves integrations over  $R$ ,  $\theta_{12}$ , and  $\Omega_3$ . The latter is obvious if one observes that  $\Phi^G$  depends on  $\Omega_3$  through the very factor  $D_{01}^{1+}(\Omega_3)$ . The remaining ones are performed using Gauss Legendre quadratures.

Apart from the few quadratures pointed out above, the numerical work involves only elementary operations of linear algebra which we complete using the standard routines from the LAPACK library [44]. The important convergence parameters in this approach are  $\ell_{\max}$ , the highest relative angular momentum included in the partial wave representation (29), and  $n$ , the number of radial basis functions (30).

In the outer region, we propagate the angular correlation pattern over  $R$  which, due to the semiclassical approximation, plays the role of a “time” variable. The numerical scheme used was developed previously within the framework of the EWRM: a detailed account of it can be found in [45] and [30,31]. Here, we only point out that the relevant parameters in this scheme are  $n_{\theta_{12}}$ , the number of points where the angular pattern is discretized;  $dt$ , the constant “time” step; and  $R_\infty$ , the end point of the propagation.

## C. Results

### 1. Numerical properties

Let us start by inspecting the numerical properties of our scheme in the illustrative case of DPI of He at  $E=6$  eV under equal energy sharing conditions.

First of all, we consider the convergence rate, assuming that convergence is obtained when the increase of any parameter leaves  $|\Phi(R_\infty, \theta_{12})|^2$  unchanged visibly. For a calculation performed with  $R_0=15$  a.u., this is achieved for  $n=15$ ,  $\ell_{\max}=5$ ,  $n_{\theta_{12}}=50$ ,  $dt=0.01$  a.u., and  $R_\infty=10^4$  a.u. The low value of  $\ell_{\max}$  is in agreement with previous analysis of experimental results based on exact and complete parametrizations of the angular dependence of the cross sections [46]. The low value of  $n$  is one more illustration of the power of Lagrange mesh techniques [41]. Accordingly, the computing times, even on our 25 Mflops down-market workstation, remain very short: 20 sec for the inner region calculation, 1 sec for the outer region propagation.

Next we must check that our results become independent of  $R_0$  as soon as the latter turns large enough for the semiclassical and adiabatic approximations to be valid in the external region. From the upper part of Fig. 1, we conclude that this independence is achieved for  $R_0 \geq 15$ . In addition, by comparing the curves  $|\phi(R_0, \theta_{12})|^2$  obtained for increasing values of  $R_0$ , we observe that the angular pattern becomes more sharply peaked around increasing values of  $\theta_{12}$ . Besides, comparing any  $|\phi(R_0, \theta_{12})|^2$  to the corresponding  $|\phi(R_\infty, \theta_{12})|^2$ , we note the same evolution of the angular pattern. The latter indeed reflects the gradual construction of the angular correlations when the two electrons move away from the ionic core. Part (a) of Fig. 1 shows that these correlations may be included as well by increasing the size of the inner region where a full quantum treatment is applied, or by propagating semiclassically over the radial coordinate. This point is discussed in more detail in [45].

The behavior of our results with respect to the gauge transformations is illustrated on the lower part of Fig. 1. We

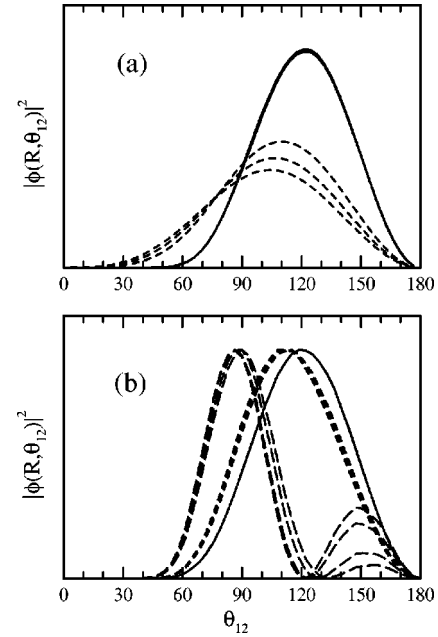


FIG. 1. (a)  $|\phi(R, \theta_{12})|^2$  at  $R_0$  (dashed lines) and at  $R_\infty$  (continuous lines) in arbitrary units versus  $\theta_{12}$  in degrees from three calculations which differ by their choice of the matching radius  $R_0$ . The three curves at  $R_0$  peak at increasing values of  $\theta_{12}$  as  $R_0$  increases from 15 to 20 and finally to 30 a.u., whereas the three curves at  $R_\infty$  coincide. (b)  $|\phi(R, \theta_{12})|^2$  at  $R_\infty$  in arbitrary units versus  $\theta_{12}$  in degrees from calculations performed in the  $L$  (long dashed lines),  $V$  (short dashed lines), and  $A$  (continuous lines) gauge, respectively. In each gauge, the calculations are reported for four different choices of the He ground-state wave function (see text). All plots refer to DPI of He at  $E_1=E_2=3$  eV.

first observe that they are gauge dependent. Next we note that there is a dependence on the helium ground-state wave function, which is very pronounced in the  $L$ , moderate in the  $V$ , and insignificant in the  $A$  gauge. All the ground-state wave functions used, however, are of a comparable accuracy, if we measure the latter, according to common practice, from the resulting value of the energy: namely,  $E = -2.9020$ ,  $-2.90244$ ,  $-2.90324$ , and  $-2.9037179$  for the two, three, six, and twenty parameter wave functions [47–49], respectively. But it is well known from photoionization studies that energy, on its own, does not provide a thorough test of the wave function: the low-amplitude parts of the latter, which contribute only little to the total energy, are particularly ill-tested. The inspection of the third-order Hylleraas wave function,

$$\begin{aligned} \Psi_0(R, \alpha, \theta_{12}) \propto & e^{-1.815R(\cos \alpha + \sin \alpha)} \\ & \times [1 + 0.29R\sqrt{1 - \sin 2\alpha \cos \theta_{12}} \\ & + 0.132R^2(\cos^2 \alpha - \sin^2 \alpha)], \end{aligned} \quad (31)$$

shows that a low amplitude is obtained if  $R$  is large, or if  $\alpha$  is close to  $\pi/4$ , or if  $\theta_{12}$  is close to 0. Accordingly, our calculations, which are performed at  $\alpha = \pi/4$ , are likely to be particularly sensitive to the inaccuracies of the ground-state wave function. Recalling from Eqs. (10) and (11) that the transition operator scales as  $R^+$ ,  $R^0$ ,  $R^-$  in the  $L$ ,  $V$ , and  $A$  gauge, respectively, we expect this sensitivity to be impor-

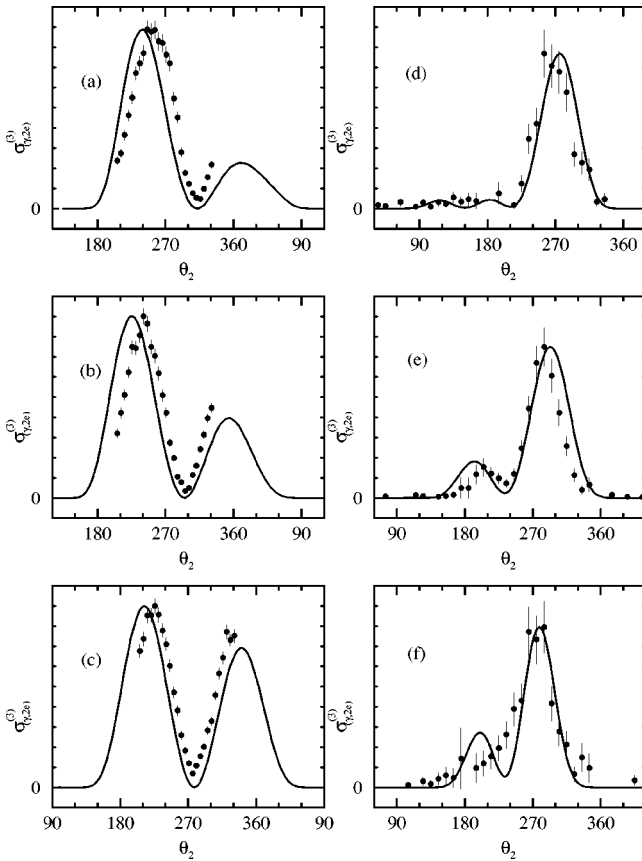


FIG. 2.  $\sigma_{(\gamma,2e)}^{(3)}$  (in arbitrary units) measured for He at  $E_1 = E_2 = E/2$  and for geometries where  $\mathbf{k}_1, \mathbf{k}_2$ , and  $\hat{\mathbf{z}}$  lie in the same plane, with  $\hat{\mathbf{z}}$  along the main axis of polarization. The direction of one electron, marked by the value of  $\theta_1 = (\hat{\mathbf{z}}, \mathbf{k}_1)$ , is fixed within a finite angular sector. The direction of the other electron sweeps the whole plane. It is marked by the angle  $\theta_2 = (\hat{\mathbf{z}}, \mathbf{k}_2)$ , which varies from  $0^\circ$  to  $360^\circ$ . Continuous line: present calculations, taking account of the opening angle for  $\theta_1$ , not for  $\theta_2$ . Points with error bars: experiments from [50] at  $E = 20$  eV with  $123.5^\circ \leq \theta_1 \leq 140.5^\circ$  (a),  $106.5^\circ \leq \theta_1 \leq 123.5^\circ$  (b), and  $89.5^\circ \leq \theta_1 \leq 106.5^\circ$  (c), from [1] at  $E = 6$  eV with  $20^\circ \leq \theta_1 \leq 40^\circ$  (d) and  $40^\circ \leq \theta_1 \leq 65^\circ$  (e), and at  $E = 1$  eV with  $40^\circ \leq \theta_1 \leq 65^\circ$  (f).

tant in the  $L$ , moderate in the  $V$ , and hopefully nonsignificant in the  $A$  gauge. This is exactly what is observed on the lower part of Fig. 1. From this analysis, we conclude that (i) we will have better chances to achieve gauge independence when we consider the general 6D case; (ii) within the present  $\alpha = \pi/4$  model, the best results are obtained in the acceleration gauge, which is the one used throughout the calculations presented below.

Another drawback of the present model is that absolute values of the cross sections cannot be obtained. This is because the  $\alpha = \pi/4$  constraint forbids populating the single escape channels, leading to a large systematic overestimation of the double escape cross sections. Accordingly, all cross sections presented below have been renormalized to experiment.

## 2. A comparison with recently measured TDCS

Figure 2 compares our calculations with the most recently measured TDCS for helium [1,50]. We have selected the

results obtained under the conditions of validity of the  $\alpha = \pi/4$  model, that is to say, at equal sharing of the excess energy between the two electrons and, by analogy with the EWRM, at low excess energy. At 20 eV excess energy, we observe a good qualitative agreement between experiment and theory, whatever the direction of  $\mathbf{k}_1$  (Fig. 2): we reproduce the double lobe experimental structure, but the angle between the two lobes is a bit too large, which indicates an underestimation of the angular correlation. This agreement seems to improve at 6 eV excess energy, as both sides of the main peak are well reproduced in part (d) of Fig. 2, although some disagreement remains in part (e). This tendency is confirmed at 1 eV, where the position and width of the main peak are obtained quantitatively [see part (f)].

The hypothesis that our model improves as energy decreases will be tested more carefully in the near future by TDCS measurements in helium at 0.1 eV [3]. For the moment, we focus on the energy domain from about 1 eV to 20 eV, where numerous measurements are available, and we turn to representative quantities, the energy evolution of which can be represented in a compact form.

The TDCS obtained at equal energy sharing is well known to factor out exactly into a *geometrical* factor, which can be set up from the Stokes parameters of the incident light and trigonometric functions of the spherical angles of the two electrons, and a *correlation factor*, depending only on the correlation angle  $\theta_{12}$  and on the total energy  $E$ , which contains all the dynamical information. Previous calculations within the Wannier mechanism [16–21] have predicted this factor to be a Gaussian function of  $(\pi - \theta_{12})$  with a full width at half maximum (FWHM)  $\Gamma(E)$  proportional to the one-fourth power of the excess energy. The values of the proportionality coefficient reported by the various authors were notably different:  $\Gamma_0 = 103, 91, 66.7^\circ (\text{eV})^{-1/4}$  in [20,18], and [16], respectively. Other authors [22,23], however, demonstrate that the Wannier mechanism itself, which is valid only in the Coulomb zone  $a_0 \leq R \leq (4Z-1)/E\sqrt{2}$  with  $a_0$  the Bohr radius, does not determine the final angular distribution. The latter can be derived, within this mechanism, only if a specific initial condition is introduced at the boundary of the inner reaction zone. The initial conditions which are implicitly assumed in the calculations leading to the Gaussian model for the correlation factor [16–21] have been found in [22] to be rather unrealistic. Despite these weaknesses of the Gaussian model, and despite the fact that the energy domain of validity of the Wannier threshold mechanism itself has never been fully established, it has become common practice to derive  $\Gamma$  values by fitting the expressions derived from the Gaussian model to the measured cross sections. We have used the same procedure here to extract  $\Gamma$  values from our *ab initio* calculations: this we do just for the sake of comparison with experimental  $\Gamma$  values; a critical comparison between our present results and the Gaussian model is reported below.

The results are summarized on part (a) of Fig. 3. The agreement between our results and experiment is excellent in the eV range, but it seems to deteriorate as the energy reaches the tens of eV range, as already noted from the angular patterns on Fig. 2. This might indicate that the energy is then high enough to liberate the electron pair from the influence of the potential surface, making deviations from

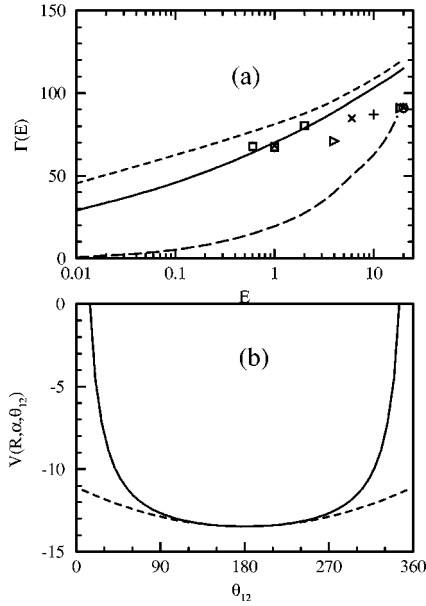


FIG. 3. (a) Full width at half maximum  $\Gamma$  of the angular correlation function in the Gaussian approximation (in degrees) versus  $E$  (in eV) on a semilogarithmic scale. Continuous line: present standard calculation. Short dashed line: present calculation with a quadratic expansion of the three-body potential with respect to  $(\pi - \theta_{12})$  in the outer region. Symbols: experimental results with crosses [1], right triangles [46], plus signs [51], circles [52], and squares [53]. The error bars of the experimental results, which are almost masked by the symbols used, have been omitted for legibility. The long dashed line is the reduced  $\chi^2$  of the fit used to extract the FWHM from our standard calculation (see text), the value of which is 1 at 0.3 eV. (b) Cut of the three-body potential (in a.u.) along  $\theta_{12}$  (in degrees) at  $R = 10$  a.u. and  $\alpha = \pi/4$ . Continuous line: exact potential. Dashed line: quadratic expansion in  $(\pi - \theta_{12})$ .

the  $\alpha = \pi/4$  ridge compatible with double escape. If this is the case, relaxing the constraint  $\alpha = \pi/4$ , either by allowing small  $\alpha$  motions around  $\pi/4$  according to the Wannier mechanism, or by letting this variable be free, should remedy this deficiency. But this disagreement could also result, to some extent, from the above-mentioned ill-defined character of  $\Gamma$ .

A quantitative estimate of the latter is given in part (a) of Fig. 3 by the reduced  $\chi^2$  associated with the best fit of the Gaussian model to our numerical calculations. Its rapid increase with increasing energy reflects the growing disagreement between the symmetric shape of the calculated  $|\Phi(R_\infty, \theta_{12})|^2$  and the asymmetric shape of the corresponding ansatz based on the Gaussian approximation, as shown in more detail on Fig. 4. The Gaussian approximation indeed seems to be acceptable below 1 eV. Below this limit, we have fitted a two-parameters  $\Gamma = \Gamma_0 E^\gamma$  law to our computed values of the FWHM and found  $\Gamma_0 = 69.7^\circ (\text{eV})^{-\gamma}$  and  $\gamma = 0.19$ . The  $\gamma$  value is within 25% of the 0.25 value predicted in [16–21]. The  $\Gamma_0$  value is close to the  $66.7^\circ (\text{eV})^{-1/4}$  value of [16]. This relative agreement, however, should be considered as accidental, given the arbitrary assumptions leading to the Gaussian model [22,23].

In order to test the Wannier assumption of small  $\theta_{12}$  motions around  $\pi$ , we have performed additional calculations with the three-body potential replaced by its quadratic ex-

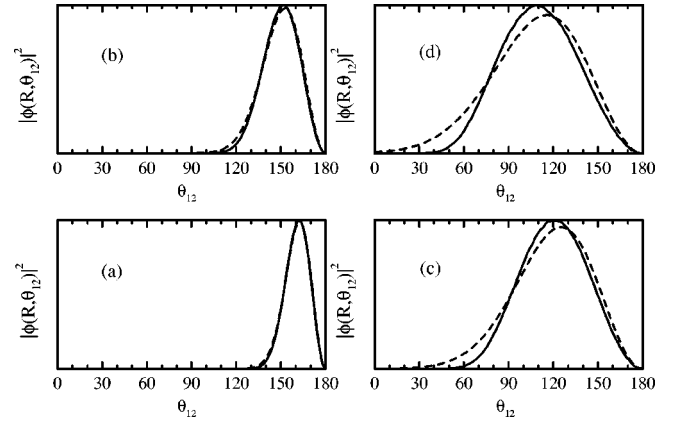


FIG. 4.  $|\phi(R, \theta_{12})|^2$  at  $R_\infty$  in arbitrary units versus  $\theta_{12}$  in degrees for increasing total energies (in eV): 0.01 (a), 0.1 (b), 10 (c), and 20 (d). Continuous lines: present calculation. Dashed lines: best fit of the Gaussian prediction to the calculated function (see text).

pansion in  $\pi - \theta_{12}$  in the external region, the inner region calculation, and hence the initial condition at  $R_0$ , being unchanged. The result is represented by the short dashed curve on part (a) of Fig. 3. The latter lies above the former continuous line throughout the energy range, with the gap between the two curves increasing on the low-energy side. This means that the quadratic approximation underestimates the angular correlation, all the worse as energy decreases. This is easily understood from the  $\theta_{12}$  cuts of the three-body potentials displayed on part (b) of Fig. 3. The exact potential lies above its quadratic approximation throughout the range of variation of  $\theta_{12}$ . The two curves remain within 10% of each other for  $|\theta_{12} - 180^\circ| \leq 120^\circ$ , but they diverge very rapidly outside this interval, with the exact potential displaying infinite repulsive walls, whereas its quadratic approximation remains finite and attractive everywhere. It is this lack of a classically forbidden region which explains the poor performance of the quadratic approximation.

Integration of the TDCS over the direction of one electron's momentum yields the doubly differential cross section (DDCS). The shape of this DDCS is well known to be controlled by the asymmetry parameter  $\beta(E)$ . The physical contents of the latter obviously are poorer than that of  $\Gamma$ . However, by contrast to  $\Gamma(E)$ ,  $\beta(E)$  is defined from first principles without relying upon any approximation. This makes it a better testing bench for our method. An excellent agreement is observed on Fig. 5 between our calculations and experiment over the entire energy range, given the experimental uncertainties. A poor performance of the quadratic approximation in  $\pi - \theta_{12}$  is observed as before.

## V. CONCLUSION

We have presented a method for computing the double photoionization cross sections of He and, more generally, of two electron atoms. This method is *ab initio*. The only approximations are the semiclassical treatment of the motion over the hyperradius  $R$ , and the local neglect of nonadiabatic radial couplings, which are applied in the external region  $R > R_0$ : the fact that our results do not depend on  $R_0$  anymore, as soon as  $R_0$  exceeds about 10 a.u., demonstrates the validity of these approximations. It is worth noting that the elec-

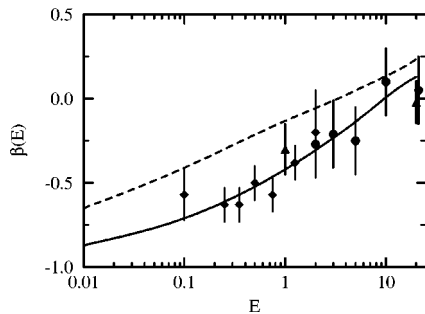


FIG. 5. Asymmetry parameter  $\beta$  versus  $E$  (in eV) on a semi-logarithmic scale. Continuous line: present standard calculation. Dashed line: present calculation with a quadratic expansion of the three-body potential with respect to  $(\pi - \theta_{12})$  in the outer region. Symbols: experimental results with diamonds [54], circles [55] as cited in [8], and up triangles [56] and [57] as cited in [56].

tronic correlations are treated nonperturbatively over the entire configuration space: this makes our method particularly valuable in the near-threshold domain where previous *ab initio* methods meet convergence problems.

We have presented an application of this general method to a model problem of reduced dimensionality: double photoionization of He with  $\alpha = \arctan(r_1/r_2)$  frozen at its saddle point value  $\pi/4$  by analogy with EWRM [30,31]. We have thus proved that the method proposed is sound and numerically effective.

The implementation of the method in the general case where  $\alpha$  is free is under progress. We anticipate that the gauge dependence, the lack of *absolute* cross sections, and the deterioration of the accuracy on the high-energy side, observed within the  $\alpha = \pi/4$  model, will be remedied by relaxing the constraint on this radial correlation angle. Detailed comparison with other existing theories will be given in this general six-dimensional case.

#### ACKNOWLEDGMENTS

We thank A. Huetz warmly for his precious support during the course of this work. We are grateful to R. Dörner and H. Bräuning for communicating the complete files of their measurements.

- 
- [1] R. Dörner, H. Bräuning, J. M. Feagin, V. Mergel, O. Jagutzki, L. Spielberger, T. Vogt, H. Khemliche, M. H. Prior, J. Ullrich, C. L. Cocke, and H. Schmidt-Böcking, *Phys. Rev. A* **57**, 1074 (1998).
- [2] V. Mergel, M. Achler, R. Dörner, K. Khayat, T. Kambara, Y. Awaya, V. Zoran, B. Nyström, L. Spielberger, J. H. McGuire, J. Feagin, J. Berakdar, Y. Azuma, and H. Schmidt-Böcking, *Phys. Rev. Lett.* **80**, 5301 (1998).
- [3] F. Rond, J. Mazeau, and A. Huetz, *J. Phys. (France) IV* **9**, 85 (1999) and A. Huetz, private communication.
- [4] A. Engels, H. Klar, and A. W. Malcherek, *J. Phys. B* **30**, L811 (1997).
- [5] J. Berakdar, *Phys. Rev. A* **53**, 2314 (1996); **54**, 1480 (1996).
- [6] M. A. Kornberg and J. E. Miraglia, *Phys. Rev. A* **48**, 3714 (1993).
- [7] E. O. Alt and A. M. Mukhamedzhanov, *Phys. Rev. A* **47**, 2004 (1993).
- [8] F. Maulbetsch and J. S. Briggs, *J. Phys. B* **26**, 1679 (1993).
- [9] M. Pont and R. Shakeshaft, *Phys. Rev. A* **51**, R2676 (1995); *J. Phys. B* **28**, L571 (1995).
- [10] J. Berakdar, *Phys. Rev. Lett.* **78**, 2712 (1997).
- [11] A. S. Kheifets and I. Bray, *Phys. Rev. A* **54**, R995 (1996).
- [12] K. W. Meyer, C. H. Greene, and B. D. Esry, *Phys. Rev. Lett.* **78**, 4902 (1997).
- [13] P. J. Marchalant and K. Bartschat, *Phys. Rev. A* **56**, R1697 (1997).
- [14] J. M. Feagin, *J. Phys. B* **29**, L551 (1996).
- [15] J. M. Rost, *Phys. Rev. A* **53**, R640 (1996).
- [16] P. L. Altick, *J. Phys. B* **18**, 1841 (1985).
- [17] D. S. F. Crothers, *J. Phys. B* **19**, 463 (1986).
- [18] J. M. Feagin, *J. Phys. B* **17**, 2433 (1984).
- [19] H. Klar, *J. Phys. B* **14**, 3255 (1981); *Z. Phys. A* **307**, 75 (1982).
- [20] A. R. P. Rau, *J. Phys. B* **9**, L283 (1976).
- [21] A. R. P. Rau and Q. Molina, *J. Phys. B* **22**, 189 (1989).
- [22] A. K. Kazansky and V. N. Ostrovsky, *J. Phys. B* **26**, 2231 (1993).
- [23] M. Gailitis and R. Peterkop, *J. Phys. B* **22**, 1231 (1989).
- [24] G. H. Wannier, *Phys. Rev.* **90**, 817 (1953).
- [25] M. S. Pindzola and F. Robicheaux, *Phys. Rev. A* **57**, 318 (1998).
- [26] M. Pont and R. Shakeshaft, *Phys. Rev. A* **51**, 494 (1995).
- [27] R. C. Forrey, Z. C. Yan, H. R. Sadeghpour, and A. Dalgarno, *Phys. Rev. Lett.* **78**, 3662 (1997).
- [28] C. W. McCurdy, T. N. Rescigno, and D. Byrum, *Phys. Rev. A* **56**, 1958 (1997).
- [29] A. K. Kazansky, V. N. Ostrovsky, and L. Yu Sergeeva, *J. Phys. B* **27**, 5197 (1994).
- [30] A. K. Kazansky and V. N. Ostrovsky, *J. Phys. B* **27**, 447 (1994).
- [31] A. K. Kazansky and V. N. Ostrovsky, *J. Phys. B* **28**, 1453 (1995); *Phys. Rev. A* **51**, 3712 (1995); *J. Phys. B* **28**, L333 (1995); **30**, 921 (1995); *Phys. Rev. A* **52**, 1775 (1995); *J. Phys. B* **30**, L835 (1995); *Phys. Rev. A* **51**, 3698 (1995).
- [32] J. H. Shirley, *Phys. Rev.* **138**, B979 (1965).
- [33] See, e.g., R. M. Potvliege and R. Shakeshaft, in *Atoms in Intense Fields*, edited by M. Gavrila (Academic, New York, 1992), pp. 373–433.
- [34] R. Peterkop, in *Theory of Ionization of Atoms by Electron Impact*, edited by D. G. Hummer (Colorado Associated University Press, Boulder, 1977).
- [35] P. G. Burke and W. D. Robb, *Adv. At. Mol. Phys.* **11**, 143 (1975).
- [36] M. Le Dourneuf, Vo Ky Lan, and J. M. Launay, *J. Phys. B* **15**, L685 (1982).
- [37] C. Bloch, *Nucl. Phys.* **4**, 503 (1957).
- [38] S. I. Nikitin and V. N. Ostrovsky, *J. Phys. B* **18**, 4349 (1985).
- [39] A. K. Bhatia and A. Temkin, *Rev. Mod. Phys.* **36**, 1050 (1964).
- [40] D. A. Varshalovich, A. N. Moskalev, and V. K. Khersonskii, *Quantum Theory of Angular Momentum* (World Scientific, Singapore, 1988).
- [41] D. Baye and P. H. Heenen, *J. Phys. A* **19**, 2041 (1986).

- [42] J. C. Light, I. P. Hamilton, and J. V. Lill, *J. Chem. Phys.* **82**, 1400 (1985).
- [43] L. Malegat and M. Vincke, *J. Phys. B* **27**, 645 (1994).
- [44] E. Anderson, Z. Bai, C. Bischof, J. Demmel, J. Dongarra, J. Du Croz, A. Greenbaum, S. Hammarling, A. McKenney, S. Ostrouchov, and D. Sorensen, *LAPACK Users' Guide* (SIAM, Philadelphia, 1992).
- [45] L. Malegat, A. Kazansky, and P. Selles, *J. Phys. B* (to be published).
- [46] L. Malegat, P. Selles, P. Lablanquie, J. Mazeau, and A. Huetz, *J. Phys. B* **30**, 263 (1997).
- [47] C. Le Sech, *J. Phys. B* **30**, L47 (1997).
- [48] E. A. Hylleraas, *Z. Phys.* **65**, 209 (1930).
- [49] J. F. Hart and G. Herzberg, *Phys. Rev.* **106**, 79 (1957).
- [50] J. P. Wightman, S. Cvejanovic, and T. J. Reddish, *J. Phys. B* **31**, 1753 (1998).
- [51] O. Schwartzkopf, B. Krässig, J. Elmiger, and V. Schmidt, *Phys. Rev. Lett.* **70**, 3008 (1993).
- [52] O. Schwartzkopf and V. Schmidt, *J. Phys. B* **28**, 2847 (1995); **29**, 1877 (1996).
- [53] G. Dawber, L. Avaldi, A. G. McConkey, H. Rojas, M. A. MacDonald, and G. C. King, *J. Phys. B* **28**, L271 (1995).
- [54] G. Dawber, R. I. Hall, A. G. McConkey, M. A. MacDonald, and G. C. King, *J. Phys. B* **27**, L341 (1994).
- [55] R. Wehlitz, F. Heiser, O. Hemmers, B. Langer, A. Menzel, and U. Becker, *Phys. Rev. Lett.* **67**, 3764 (1991).
- [56] H. Braüning, R. Dörner, C. L. Cocke, M. H. Prior, B. Krässig, A. Braüning-Demian, K. Carnes, S. Dreuil, V. Mergel, P. Richard, J. Ullrich, and H. Schmidt-Böcking, *J. Phys. B* **30**, L649 (1997).
- [57] R. Dörner, J. M. Feagin, C. L. Cocke, H. Braüning, O. Jagutzki, M. Jung, E. P. Kanter, H. Khemliche, S. Kravis, V. Mergel, M. H. Prior, H. Schmidt-Böcking, L. Spielberger, J. Ullrich, M. Unversagt, and T. Vogt, *Phys. Rev. Lett.* **77**, 1024 (1996).